한국소음진동공학회 2008년 추계학술대회논문집, pp.256~263

굽힘 및 비틀림 연성 효과를 고려한 대형 풍력 터빈 블레이드의 강제 진동 및 하중 해석

Forced Vibration and Loads Analysis of Large-scale Wind Turbine Blades Considering Blade Bending and Torsion Coupling

김경택† · 박종포* · 이종원**

Kyung-Taek Kim, Jong-Po Park and Chong-Won Lee

Key words: wind turbine blade(풍력 터빈 블레이드), coupled vibration(연성 진동), aeroelastic modelling(공탄성 모형화)

ABSTRACT

The assumed modes method is developed to derive a set of linear differential equations describing the motion of a flexible wind turbine blade and to propose an approach to investigate the forced responses result from various wind excitations. In this work, we have adopted Euler beam theory and considered that the root of the blade is clamped at the rigid hub. And the aerodynamic parameters and forces are determined based on Blade Element Momentum (BEM) theory and quasi-steady airfoil aerodynamics. Numerical calculations show that this method gives good results and it can be used for modeling and the forced vibration analysis including the coupling effect of wind-turbine blades, as well as turbo-machinery blades, aircraft propellers or helicopter rotor blades which may be considered as straight non-uniform beams with built-in pre-twist.

1. INTRODUCTION

For economic reasons, wind turbines of today are being designed to increase the rotor diameter as much as possible [1],[2],[3]. As a consequence, the wind turbine blades are being designed larger and more flexible than ever before. And the flexibility of the blades has continued to increase to the point where their dynamic behavior could cause serious structural problems, such as resonance or instability [4]. Accordingly, dynamic characteristics of the wind turbine blades have become much more important in modern wind turbine design and loads analysis. For this season, the present work is devoted to developing an accurate and efficient aeroelastic response prediction method for loads analysis of large-scale wind turbines with flexible blades.

Many researches have been performed on structural model of non-uniform beam with built-in pre-twist. The differential equations of motion for coupled bending and torsion of a pre-twisted non-uniform rotor blade were derived [5]. Hodges and Dowell [6] also developed the nonlinear partial differential equations of motion for a pre-twisted helicopter blade. Kallesøe [7] extended Hodges and Dowell's equations of motion, by including the effect of gravity, pitch action and varying rotor speed.

† Kyung-Taek Kim; NoViC, KAIST
E-mail : taeks88@kaist.ac.kr
Tel : (042) 869-3065, Fax : (042) 869-8220
* Doosan Heavy Industries & Construction
** NoViC, KAIST

However, since these differential equations of motion can hardly be solved exactly, either the solutions to special sub-cases of the above problem or approximate solutions have been attempted by many investigators. The integrating matrix method has been introduced to determine the natural vibration characteristics of rotor blade [8]. Murthy [9],[10] used the transmission matrix method to obtain the solutions for the general case. Besides, reference [11] contains a review of several approximate methods such as the Myklestad method, the Galerkin method, the Rayleigh-Ritz method, the finite element method (FEM), etc.

Among the previous methods cited above, FEM is widely used for the structural, fluid flow and heat transfer areas and it may produce quite useful results for realistic modeling of wind turbine rotors with anisotropic blades. But, due to the high computational cost and the complicated final system matrix, the FEM is found to be not suitable for preliminary design, performance optimization and controller design [12].

In the present paper, the assumed mode method that coalesces with the Lagrange's equation is developed to derive the mathematical model that describes the coupled bending and torsional vibration of the wind turbine blades whose lower modes are of interest. A feature of the assumed mode method is that it is computationally efficient and that it would offer easy understanding of the physical characteristics of the system, not requiring the large number of degrees of freedom as required in FEM [10]. And it is well-known that the Blade Element

Momentum (BEM) is the most common engineering theory for computation of aerodynamic forces and most wind turbine structural design codes adopt the BEM in blade aerodynamic performance simulation [13]. For this reason, the aerodynamic forces are determined based on BEM theory in this work.

2. ANALYSIS MODEL

Consider a rotating inextensible wind turbine blade as shown in Fig. 2-1. It is assumed that the blade is a rotating pre-twisted beam with non-uniform cross-section and the root of the blade is clamped at the rigid hub of radius h and the shear and the elastic centre of the blade are assumed to coincide. Since the wind turbine blades can be well represented as a slender beam and only the low frequency vibration modes are of interest, we have adopted Euler beam theory not taking the anisotropic and warping effects into account. But, if necessary, the elastic energy could instead be described with the more accurate and detailed beam theory without difficulty.

2.1 Coordinate System

Figure 2-1 shows the blade rotating at Ω in the rotor plane. The Z-axis of the reference frame, O-XYZ whose origin is located at the center of the rotor hub, points upwind and the X, Y-axis spans the rotor plane, with the X-axis pointing downward. Since the tower top and yaw position are assumed fixed, the reference frame O-XYZ becomes an inertial frame which is appropriate for representing the total forces and moments on the rotor.

The reference frame R-xyz is attached at the blade root and rotates with the blade, such that the x- and z-axes are aligned with the pitch axis of the blade and the Z-axis, respectively. Then the elastic deformations of blades are defined simply as the motions relative to the rotating reference frame R-xyz and the forces and moments acting on the blades can be resolved in a rotating coordinate system with respect to the local blade cross-section. This approach is practical when the vibrations of the blades themselves are considered.

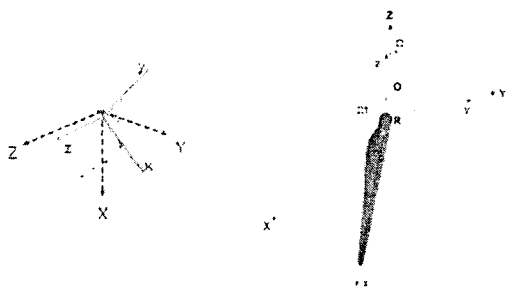

Figure 2-1. Global coordinate system: inertial frame O-XYZ and rotating frame R-xyz

An arbitrary cross-section of the blade looking outward along the x-axis is shown in Fig. 2-2. The reference frame P-$\xi\eta\zeta$ is fixed at the elastic axis of the blade. The η- and ζ-axes, which are the elastic principle axes of the blade section, are rotated by the angle of $\beta+\theta_p+\Phi$, relative to the x-y plane, where θ_p and β are the blade pitch angle and the pre-twist angle, respectively, and Φ is the time-dependent torsional deflection angle. The position of the elastic axis P in the reference frame R-xyz is given by (x, v, w), where v and w are the displacement from the undeformed position in the y- and z-direction, respectively. The independent variables t and x are the time and distance from the root of the blade measured along the elastic axis. The centre of mass is assumed to be located at G and the mass eccentricity from the elastic axis is given by e_η and e_ζ in the η- and ζ-direction, respectively.

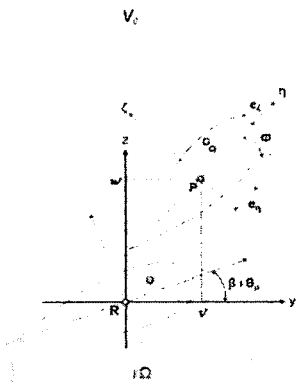

Figure 2-2. Local coordinate system: blade fixed frame P-$\xi\,\eta\,\zeta$

2.2 Energy Functions and Virtual Work

2.2.1 Kinetic Energy

The positions of the point G before and after deformation in the cross-sectional plane are shown in Fig. 2-2. In the reference frame, R-xyz, the kinetic energy of the blade can be written as

$$KE = \frac{1}{2}\int_0^l [m\,\mathbf{V}_G \cdot \mathbf{V}_G + J_p\,\boldsymbol{\omega}_\phi \cdot \boldsymbol{\omega}_\phi]dx \qquad (2\text{-}1)$$

where $\mathbf{V}_G$ is the linear velocity vector of the mass center G, $\boldsymbol{\omega}_G$ is the angular velocity vector of the reference frame P-$\xi\,\eta\,\zeta$ with respect to the frame O-XYZ, l is the blade length and, m and J_p are the distributed mass and the mass moment of inertia of the blade, respectively.

2.2.2 Potential Energy

The elastic strain energy of the pre-twisted blade undergoing the coupled flap-wise bending, lead-lag bending, and pitch-wise torsion is can be written a

$$PE_E = \frac{1}{2}\int_0^l [EI_y \cdot (w'')^2 + EI_z \cdot (v'')^2 ... \\ ... + 2EI_{zy} \cdot w'' \cdot v'' + GJ \cdot (\phi')^2]dx \quad (2\text{-}2)$$

where EI_y, EI_z and EI_{zy} are the flexural rigidity, and GJ is the torsional rigidity of the blade.

The potential energy associated with the centrifugal stress and gravity fields measured in the rotating frame *R-xyz* is described as

$$PE_{C+G} = \frac{1}{2}\int_0^l [T \cdot \{(w')^2 + (v')^2\} + 2mg \cdot sin(\Omega t) ... \\ .... \cdot \{v - (e_\eta sin\theta + e_\varsigma cos\theta) \cdot \phi\}]dx \quad (2\text{-}3)$$

where T is the axial force component of the blade, given by

$$T = \int_x^l m\{(x+h)\Omega^2 + g cos(\Omega t)\}dx \quad (2\text{-}4)$$

From Eqs. (2) and (3), the total potential energy of the blade is given by

$$PE = PE_E + PE_{C+G} \quad (2\text{-}5)$$

2.2.3 Virtual Work

Figure 2-3 and 2-4 show the velocity and aerodynamic force components in the plane of a blade cross-section at distance of x from the blade root. According to the BEM theory, each blade element is modeled as a two-dimensional airfoil meaning that span-wise flow is neglected and thus, the forces acting on the blade element are essentially two-dimensional [1], [2].

From Fig. 2-3, the resultant wind velocity relative to the blade element can be written as

$$V_{rel} = \sqrt{\{V_0(1-a) + \dot{w}\}^2 + \{\Omega(x+h)(1+a') + \dot{v}\}^2} \quad (2\text{-}6)$$

where a and a' are the axial and tangential induction factors whose thorough derivation is given in most wind turbine design handbooks [2].

The aerodynamic forces acting on the blades are governed by the geometry of the flow, or better known as the angle of attack. Since the blade element includes a torsional degree of freedom, the angle of attack is determined by the inflow velocity and the velocity of the blade's motion at the collocation point *CP*, which is located in the three-quarter chord length from the leading edge of the airfoil [4]. Thus the angle of attack α is then given by

$$\alpha = tan^{-1}\left(\frac{V_0(1-a) + \dot{w} - c(3/4 - a_{pa})cos(\phi+\theta)\dot{\phi}}{\Omega(x+h)(1+a') + \dot{v} + c(3/4 - a_{pa})sin(\phi+\theta)\dot{\phi}}\right) ... \\ ... - \phi - \theta \quad (2\text{-}7)$$

where c represents the chord length and the non dimensional parameter a_{pa} defines the position of the pitch axis (elastic axis, shear centre position) of the blade element.

The relative wind velocity and the angle of attack give rise to aerodynamic forces on the blade element described as

$$F_l = \frac{1}{2} \cdot \rho \cdot V_{rel}^2 \cdot c \cdot C_l \quad (2\text{-}8)$$

$$F_d = \frac{1}{2} \cdot \rho \cdot V_{rel}^2 \cdot c \cdot C_d \quad (2\text{-}9)$$

$$M_m = \frac{1}{2} \cdot \rho \cdot V_{rel}^2 \cdot c^2 \cdot C_m \quad (2\text{-}10)$$

where F_l, F_d, M_m are aerodynamic lift force, drag force, pitching moment and C_l, C_d, C_m are the lift, drag and pitching moment coefficients, which are functions of the angle of attack, respectively.

As shown in Fig. 2-4 (b), these aerodynamic forces can be written in the reference frame *R-xyz* to represent the thrust and the rotor driving torque, which are the dominant forces for turbine design.

$$F_w = -F_l cos(\alpha+\theta+\phi) - F_d sin(\alpha+\theta+\phi) \quad (2\text{-}11)$$

$$F_v = F_l sin(\alpha+\theta+\phi) - F_d cos(\alpha+\theta+\phi) \quad (2\text{-}12)$$

$$M_p = -M_m + F_w\{c\,a_{ac} cos(\theta+\phi)\} - F_v\{c\,a_{ac} sin(\theta+\phi)\} \quad (2\text{-}13)$$

According to the virtual work principle, the virtual work done by the aerodynamic forces can be derived as follows

$$\delta W = \int_0^l [\delta w F_w + \delta v F_v + \delta\phi M_p]dx \quad (2\text{-}14)$$

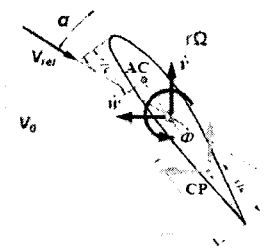

Figure 2-3. Velocity components in the plane of arbitrary blade cross-section

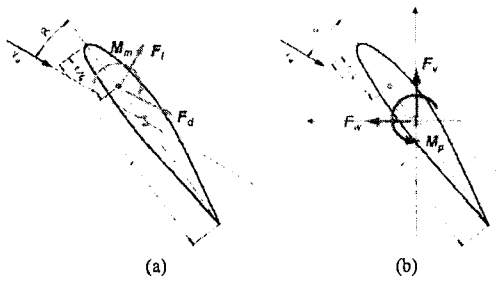

Figure 2-4. Aerodynamic forces acting on the arbitrary blade cross-section

2.3 Assumed Modes Method

The motion of every substructure may be approximated by a weighted superposition of admissible functions [15]. As admissible functions, the mode shapes obtained from the analytical solutions of the non-rotating uniform cantilever beam can be used [14].

$$w(x,t) \cong \mathbf{W}^{\mathrm{T}}(x)\,\mathbf{q}_w(t) \tag{2-15}$$

$$v(x,t) \cong \mathbf{V}^{\mathrm{T}}(x)\,\mathbf{q}_v(t) \tag{2-16}$$

$$\phi(x,t) \cong \mathbf{\Phi}^{\mathrm{T}}(x)\,\mathbf{q}_\phi(t) \tag{2-17}$$

where $\mathbf{W}$, $\mathbf{V}$ and $\mathbf{\Phi}$ are the column vectors consisting of admissible functions, which describe the flap-wise bending, lead-lag bending and pitch-wise torsional motions in the rotating frame, *R-xyz*, and, $\boldsymbol{q}_w$, $\boldsymbol{q}_v$ and $\boldsymbol{q}_\Phi$ are the column vectors consisting of the corresponding time-dependent generalized coordinates.

2.4 Equations of Motion

Linearization of the virtual work using Taylor series expansion and applying the assumed modes method that coalesces with the Lagrange's equation yield a set of linear differential equations for the blade and these equations of motion can be expressed as the following matrix form.

$$\mathbf{M}\ddot{\mathbf{x}} + \mathbf{C}\dot{\mathbf{x}} + \mathbf{K}\mathbf{x} = \mathbf{U}_0 + \mathbf{F}_0 \tag{2-18}$$

where $\mathbf{F}_0$ is the coordinate independent generalized force vector which results from the aerodynamic forces. The other coordinate independent vector, $\mathbf{U}_0$ arises from the mass eccentricity and gravitational effect of the rotating blade. The expressions of the element matrices are given in Appendix.

The equations of motion (2-18) show that the flap-wise and lead-lag vibrations are elastically coupled each other due to the angle θ, which includes the pre-twist and the pitch angle of the blade, and the bending and torsional vibrations are dynamically coupled due to the presence of mass eccentricity, (e_η, e_ζ). In addition, it also shows that the aerodynamic forces are coupled with the generalized coordinates and contribute to the damping and stiffness matrices which could cause aeroelastic instability [4].

The relatively simple structure of the equations of motion makes them suitable for modeling and vibration analysis including the coupling effect of wind turbine blades, as well as turbo-machinery blades, aircraft propellers or helicopter rotor blades which may be considered as straight non-uniform beams with built-in pre-twist.

3. NUMERICAL EXAMPLE

In order to validate the present formulation, demonstrate the effectiveness of the presented method and examine the wind turbine blade loadings during operation, the forced vibration analysis is performed on a typical pre-twisted wind turbine blade with a non-uniform cross section and the cantilever boundary conditions at the root.

To describe deflections of the blade, a total of 24 admissible functions (8 admissible functions for each of the deflection variables: w, v, Φ) were used and mode shapes of the non-rotating uniform beam with clamped-free boundary condition were used as the admissible functions.

3.1 Test Blade Configurations

The blade of virtual 5MW variable-speed, pitch-regulated wind turbine designed by National Renewable Energy Laboratory (NREL) [16] is used for numerical simulation. This turbine has a 126-m-diameter rotor with three 61.5-m-long pre-twisted blades and the rated rotor speed is 12.1 rpm. Figure 2-5 describes the test blade with the positions of the elastic centre and the centre of gravity. It shows that since the centre of gravity lies aft of the elastic axis, the bending and torsion coupled motion would be expected.

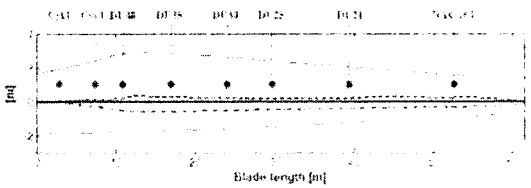

Figure 3-1 Configuration of the NREL 5MW wind turbine blade: ----, mass centre; ——, pitch axis (elastic centre); — · —, aerodynamic centre

3.2 Forced Vibration Analysis

To demonstrate the dynamic response of the test blade, standard wind profiles as defined in the IEC61400-1 [17] are applied to the blade model on the rated wind condition and the blade tip displacements and blade root moments are examined. During the entire simulation, the mean wind speed at hub and the rotor speed are taken as 11.2 m/s and 12.1 r.p.m., respectively.

3.2.1 Response to Steady Mean Wind

If a steady, uniform flow entering the area swept by the rotor is assumed, the rotor blades of a horizontal-axis rotor are subjected to steady-state aerodynamic forces as shown Fig. 3-2. The lead-lag bending moment on the rotor blades are the result of the tangential force distribution, whereas the thrust distribution is responsible for the flap-wise blade bending moments.

3.2.2 Response to Steady Wind Shear

The wind speed gradient with elevation is known as wind shear and it is often modeled by a simple power law [19] as

$$V_{WS} = V_{hub}\left(z / z_{hub}\right)^{E} \tag{3-1}$$

where V_{hub} means the wind speed at hub elevation. Z and Z_{hub} are the elevation above ground level and the elevation of the rotor hub, respectively. E is the empirical wind shear exponent and it is specified by international standard, IEC 61400-1 [17] as a conservative value of 0.2.

The steady wind shear produces a cyclic variation in the wind speed to a rotating blade element. The variation of blade tip displacements and blade root bending moments with azimuth due to wind shear is illustrated in Fig. 3-3. The flap-wise displacement and bending moment are almost a sinusoidal function of azimuth varying with wind speed.

3.2.3 Response to Tower Shadow

Blocking the air flow by the tower results in region of reduced wind speed both up-wind and down-wind side of the tower. The up-wind velocity deficits of tubular tower can be modeled using potential flow theory [2] and the inflow velocity is given by

$$V_{TS} = V_{hub}\left(1 - \frac{(D/2)^2(x^2 - y^2)}{(x^2 + y^2)^2}\right) \tag{3-2}$$

where D (=5m) is the tower diameter, and y and x are the lateral coordinates and the distance of rotor plane with respect to the tower centre. Figure 3-4 shows the blade tip displacements and the variation of lead-lag and flap-wise root bending moments with azimuth during operation. Note that the dip in flap-wise bending moment is observed and more severe than lead-lag bending moment.

3.2.4 Response to wind shear and tower shadow with gravity and centrifugal effect

As shown in Fig.3-5, the lead-lag bending moment is almost a sinusoidal function of azimuth, being dominated by the gravity loading due to weight of the blade which changes direction once per revolution. The mean value for lead-lag moment is not zero because of the mean positive aerodynamic torque developed by the blade. A slight distortion on the lead-lag bending moment line is observed, because of the variation of aerodynamic torque due to wind shear with the tower shadow effect, and the flap-wise blade vibration.

The flap-wise moment is always positive due to the aerodynamic thrust on the blade. Figure 3-5 shows a relatively small load at 0° azimuth (bottom dead centre) than at 180° in the flap-wise bending moment. The load variation with azimuth results from the wind shear. And a sharp dip at 0° is also visible and this is due to the tower shadow effect.

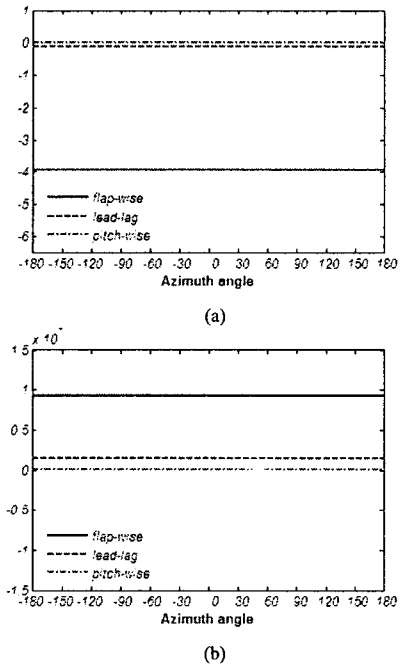

Figure 3-2. (a) Blade tip displacements and (b) blade root moments with azimuth due to steady mean wind

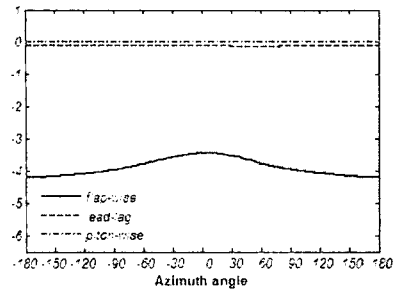

(a)

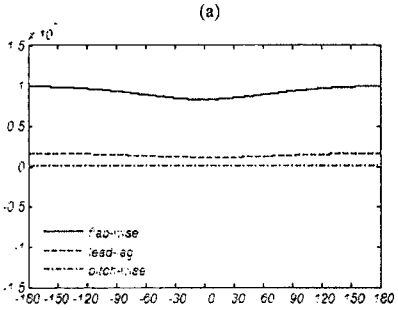

(b)

Figure 3-3. (a) Blade tip displacements and (b) blade root moments with azimuth due to steady wind shear

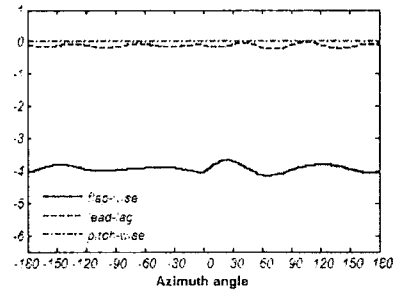

(a)

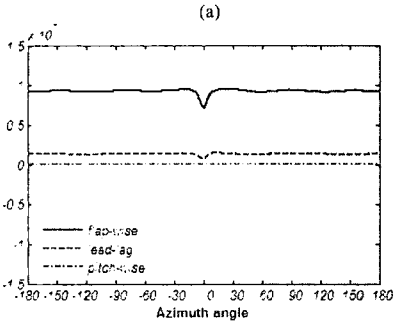

(b)

Figure 3-4. (a) Blade tip displacements and (b) blade root moments with azimuth due to steady mean wind and tower shadow effect

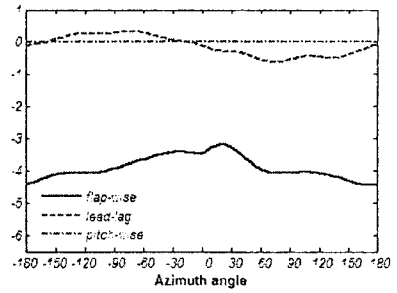

(a)

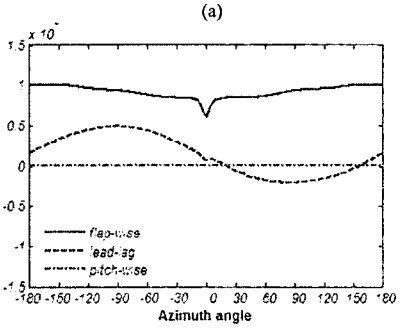

(b)

Figure 3-5. (a) Blade tip displacements and (b) blade root moments with azimuth due to shear and tower shadow with gravity and centrifugal effect

4. CONCLUSION

A set of ordinary differential equations, governing the coupled dynamic motion of a flexible wind turbine blade, and aerodynamic forces, acting on the blade have been formulated by using assumed mode method. From this blade aeroelastic model, the forced response and the root moment of the blade are examined by applying typical steady wind profiles. The results have shown that the forced response and the loads of the blade reflect corresponding wind characteristics well and the present model successfully captures the fundamental structural and aerodynamic characteristics of the blade.

ACKNOWLEDGEMENTS

This work was supported by a grant from Doosan Heavy Industries & Construction, Korea.

REFERENCES

[1] D. A. Spera, *Wind Turbine Technology*, ASME Press, New York, NY, 1994.

[2] T. Burton, et al., *Wind energy handbook*, John Wiley & Sons, LTD, Baffins Lane, Chichester, 41-91, (2001)

[3] P. S. Veers, et al. "Trends in the Design, Manufacture and Evaluation of Wind Turbine Blades", *Wind Energ.*6, 245-259 (2003).

[4] M. H. Hansen, "Aeroelastic Instability Problems for Wind Turbines", *Wind Energ.*10, 551-577 (2007).

[5] J. C. Houbolt, G. W. Brooks, "Differential Equations of Motion for Combined Flapwise Bending, Chordwise Bending, and Torsion of Twisted Nonuniform Rotor Blades", NACA Report 1346 (1958).

[6] D. H. Hodges, E. H. Dowell, "Nonlinear Equations of Motion for the Elastic Bending and Torsion of Twisted Nonuniform Rotor Blades", Technical Report, TN D-7818, NASA, (1974).

[7] B. S. Kallesøe, "Equation of Motion for Rotor Blade, Including Gravity, Pitch Action and Rotor Speed Variations", *Wind Energ.*10, 209-230 (2007).

[8] W. F. Hunter, "The Integrating Matrix Method for Determining the Natural Vibration Characteristics of Propeller Blades", Technical Report, NASA TN D-6064 (1970).

[9] V. R. Murthy, "Dynamic Characteristics of Rotor Blades", *Journal of Sound and Vibration* 49(4), 483-500 (1976).

[10] V. R. Murthy, A. M. Joshi, "Free Vibration Characteristics of Multiple Load Path Blades by the Transfer Matrix Method", *Journal of the American Helicopter Society* 31(5), 43-50 (1986).

[11] R. L. Bielawa, *Rotary wing structural dynamics and aeroelasticity*, AIAA Education Series, Washington, D.C., 63-109 (1992)

[12] D. H. Lee, D. H. Hodge and M. J. Patil, "Multi-flexible-body Dynamic Analysis of Horizontal Axis Wind Turbine", *Wind Energ.*5, 281-300 (2002).

[13] J. Jonkman, et al. "Offshore Code Comparison Collaboration within IEA Wind Annex XXIII: Phase II results regarding monopile foundation modeling", *IEA European Offshore Wind Conference*, Berlin, Germany, December 4–6, (2007).

[14] S. B. Chun, C. W. Lee. "Vibration Analysis of Shaft-bladed Disk System by Using Substructure Synthesis and Assumed Mode Method", *Journal of Sound and Vibration* 189(5), 587-608 (1996).

[15] L. Meirovitch, *Analytical methods in vibrations*, London, Macmillan, 542-543, (1967).

[16] J. Jonkman, NRELOffshrBsline5MW, Technical Report, NREL/NWTC, Golden, CO, (2005).

[17] IEC. *Wind turbine generator systems –Part 1: Safety requirements*, International Standard 61400-1 Second edition, International Electrotechnical Commission, (1999).

[18] K. T. Kim and C. W. Lee, "Coupled Bending and Torsional Vibration Analysis of Flexible Wind Turbine Blades by Using Assumed Modes Method", *15th International Congress on Sound and Vibration*, Daejeon, Korea, July 6-10, (2008).

APPENDIX

Element matrices

$$\mathbf{M}_{11}=\mathbf{A}_1 \quad \mathbf{C}_{11}=-\int_0^l \bar{B}_2\,dx \quad \mathbf{K}_{11}=\mathbf{A}_8$$

$$\mathbf{M}_{12}=\mathbf{0} \quad \mathbf{C}_{12}=-\int_0^l \bar{B}_3\,dx \quad \mathbf{K}_{12}=\mathbf{A}_{11}$$

$$\mathbf{M}_{13}=\mathbf{A}_5 \quad \mathbf{C}_{13}=-\int_0^l \bar{B}_4\,dx \quad \mathbf{K}_{13}=-\int_0^l \bar{B}_5\,dx$$

$$\mathbf{M}_{21}=\mathbf{0} \quad \mathbf{C}_{21}=-\int_0^l \bar{B}_7\,dx \quad \mathbf{K}_{21}=\mathbf{A}_{11}^{\mathrm{T}}$$

$$\mathbf{M}_{22}=\mathbf{A}_2 \quad \mathbf{C}_{22}=-\int_0^l \bar{B}_8\,dx \quad \mathbf{K}_{22}=\mathbf{A}_9$$

$$\mathbf{M}_{23}=-\mathbf{A}_4 \quad \mathbf{C}_{23}=-\int_0^l \bar{B}_9\,dx \quad \mathbf{K}_{23}=\mathbf{A}_{12}-\int_0^l \bar{B}_{10}\,dx$$

$$\mathbf{M}_{31}=\mathbf{A}_5^{\mathrm{T}} \quad \mathbf{C}_{31}=-\int_0^l \bar{B}_{12}\,dx \quad \mathbf{K}_{31}=\mathbf{0}$$

$$\mathbf{M}_{32}=-\mathbf{A}_4^{\mathrm{T}} \quad \mathbf{C}_{32}=-\int_0^l \bar{B}_{13}\,dx \quad \mathbf{K}_{32}=\mathbf{A}_{12}^{\mathrm{T}}$$

$$\mathbf{M}_{33}=\mathbf{A}_3 \quad \mathbf{C}_{33}=-\int_0^l \bar{B}_{14}\,dx \quad \mathbf{K}_{33}=\mathbf{A}_{10}-\int_0^l \bar{B}_{15}\,dx$$

$$\mathbf{U}_1=\mathbf{0} \quad \mathbf{U}_2=\mathbf{A}_{13} \quad \mathbf{U}_3=-\mathbf{A}_{14}$$

$$\mathbf{F}_1=\int_0^l \bar{B}_1\,dx \quad \mathbf{F}_2=\int_0^l \bar{B}_6\,dx \quad \mathbf{F}_3=\int_0^l \bar{B}_{11}\,dx$$

$$A_1=\int_0^l [m\mathbf{W}\mathbf{W}^{\mathrm{T}}]dx$$

$$A_2=\int_0^l [m\mathbf{V}\mathbf{V}^{\mathrm{T}}]dx$$

$$A_3=\int_0^l [\{m(e_\eta^{\,2}+e_\varsigma^{\,2})+J_P\}\mathbf{\Phi}\mathbf{\Phi}^{\mathrm{T}}]dx$$

$$A_4=\int_0^l [m(e_\eta \sin\theta+e_\varsigma \cos\theta)\mathbf{V}\mathbf{\Phi}^{\mathrm{T}}]dx$$

$$A_5=\int_0^l [m(e_\eta \cos\theta-e_\varsigma \sin\theta)\mathbf{W}\mathbf{\Phi}^{\mathrm{T}}]dx$$

$$A_8=\int_0^l [EI_y\mathbf{W}''\mathbf{W}''^{\mathrm{T}}+T\mathbf{W}'\mathbf{W}'^{\mathrm{T}}]dx$$

$$A_9=\int_0^l [-m\Omega^2\mathbf{V}\mathbf{V}^{\mathrm{T}}+EI_z\mathbf{V}''\mathbf{V}''^{\mathrm{T}}+T\mathbf{V}'\mathbf{V}'^{\mathrm{T}}]dx$$

$$A_{10}=\int_0^l [-\Omega^2\{m(e_\eta \sin\theta+e_\varsigma \cos\theta)^2+J_P\}\mathbf{\Phi}\mathbf{\Phi}^{\mathrm{T}}+GJ\mathbf{\Phi}'\mathbf{\Phi}'^{\mathrm{T}}]dx$$

$$A_{11}=\int_0^l [EI_{zy}\mathbf{W}''\mathbf{V}''^{\mathrm{T}}]dx$$

$$A_{12}=\int_0^l [m\Omega^2(e_\eta \sin\theta+e_\varsigma \cos\theta)\mathbf{V}\mathbf{\Phi}^{\mathrm{T}}]dx$$

$$A_{13}=\int_0^l [\{m\Omega^2(e_\eta \cos\theta-e_\varsigma \sin\theta)-mg\sin\Omega t\}\mathbf{V}]dx$$

$$A_{14}=\int_0^l [\{m\Omega^2(e_\eta \sin\theta+e_\varsigma \cos\theta)(e_\eta \cos\theta-e_\varsigma \sin\theta)\ldots$$
$$\ldots-mg\sin\Omega t\,(e_\eta \sin\theta+e_\varsigma \cos\theta)\}\mathbf{\Phi}]dx$$

$$\bar{B}_1 = -\tfrac{1}{2}\rho c[\{V_0(1-a)\}^2 + \{\Omega(x+h)(1+a')\}^2]...$$
$$...\cdot\{\tilde{C}_l cos\tilde{\psi} + \tilde{C}_d sin\tilde{\psi}\}$$

$$\bar{B}_2 = -\tfrac{1}{2}\rho c[2\{V_0(1-a)\}]\cdot[\tilde{C}_l cos\tilde{\psi} + \tilde{C}_d sin\tilde{\psi}]...$$
$$...-\tfrac{1}{2}\rho c[\{V_0(1-a)\}^2 + \{\Omega(x+h)(1+a')\}^2]...$$
$$...\cdot[(\tilde{C}_{l(\alpha)} + \tilde{C}_d)cos\tilde{\psi} + (\tilde{C}_{d(\alpha)} - \tilde{C}_l)sin\tilde{\psi}]\tilde{\alpha}_{(w)}$$

$$\bar{B}_3 = -\tfrac{1}{2}\rho c[2\{(x+h)\Omega(1+a')\}]\cdot[\tilde{C}_l cos\tilde{\psi} + \tilde{C}_d sin\tilde{\psi}]...$$
$$...-\tfrac{1}{2}\rho c[\{V_0(1-a)\}^2 + \{\Omega(x+h)(1+a')\}^2]...$$
$$...\cdot[(\tilde{C}_{l(\alpha)} + \tilde{C}_d)cos\tilde{\psi} + (\tilde{C}_{d(\alpha)} - \tilde{C}_l)sin\tilde{\psi}]\tilde{\alpha}_{(v)}$$

$$\bar{B}_4 = -\tfrac{1}{2}\rho c[\{V_0(1-a)\}^2 + \{\Omega(x+h)(1+a')\}^2]$$
$$...\cdot[(\tilde{C}_{l(\alpha)} + \tilde{C}_d)cos\tilde{\psi} + (\tilde{C}_{d(\alpha)} - \tilde{C}_l)sin\tilde{\psi}]\tilde{\alpha}_{(\phi)}$$

$$\bar{B}_5 = \tfrac{1}{2}\rho c[\{V_0(1-a)\}^2 + \{\Omega(x+h)(1+a')\}^2]...$$
$$...\cdot\{\tilde{C}_{l(\alpha)} cos\tilde{\psi} + \tilde{C}_{d(\alpha)} sin\tilde{\psi}\}$$

$$\bar{B}_6 = \tfrac{1}{2}\rho c[\{V_0(1-a)\}^2 + \{\Omega(x+h)(1+a')\}^2]...$$
$$...\cdot\{\tilde{C}_l sin\tilde{\psi} - \tilde{C}_d cos\tilde{\psi}\}$$

$$\bar{B}_7 = \tfrac{1}{2}\rho c[2\{V_0(1-a)\}]\cdot[\tilde{C}_l sin\tilde{\psi} - \tilde{C}_d cos\tilde{\psi}]...$$
$$...+\tfrac{1}{2}\rho c[\{V_0(1-a)\}^2 + \{\Omega(x+h)(1+a')\}^2]...$$
$$...\cdot[(\tilde{C}_{l(\alpha)} + \tilde{C}_d)sin\tilde{\psi} - (\tilde{C}_{d(\alpha)} - \tilde{C}_l)cos\tilde{\psi}]\tilde{\alpha}_{(w)}$$

$$\bar{B}_8 = \tfrac{1}{2}\rho c[2\{\Omega(x+h)(1+a')\}]\cdot[\tilde{C}_l sin\tilde{\psi} - \tilde{C}_d cos\tilde{\psi}]...$$
$$...+\tfrac{1}{2}\rho c[\{V_0(1-a)\}^2 + \{\Omega(x+h)(1+a')\}^2]...$$
$$...\cdot[(\tilde{C}_{l(\alpha)} + \tilde{C}_d)sin\tilde{\psi} - (\tilde{C}_{d(\alpha)} - \tilde{C}_l)cos\tilde{\psi}]\tilde{\alpha}_{(v)}$$

$$\bar{B}_9 = \tfrac{1}{2}\rho c[\{V_0(1-a)\}^2 + \{\Omega(x+h)(1+a')\}^2]...$$
$$...\cdot[(\tilde{C}_{l(\alpha)} + \tilde{C}_d)sin\tilde{\psi} - (\tilde{C}_{d(\alpha)} - \tilde{C}_l)cos\tilde{\psi}]\tilde{\alpha}_{(\phi)}$$

$$\bar{B}_{10} = \tfrac{1}{2}\rho c[\{V_0(1-a)\}^2 + \{\Omega(x+h)(1+a')\}^2]...$$
$$...\cdot\{\tilde{C}_{d(\alpha)} cos\tilde{\psi} - \tilde{C}_{l(\alpha)} sin\tilde{\psi}\}$$

$$\bar{B}_{11} = -\tfrac{1}{2}\rho c^2[\{V_0(1-a)\}^2 + \{\Omega(x+h)(1+a')\}^2]\cdot\tilde{C}_m...$$
$$...+\bar{B}_1 ca_{ac} cos\theta - \bar{B}_0 ca_{ac} sin\theta$$

$$\bar{B}_{12} = -\tfrac{1}{2}\rho c^2[2\{V_0(1-a)\}]\tilde{C}_m - \tfrac{1}{2}\rho c^2[\{V_0(1-a)\}^2...$$
$$...+\{\Omega(x+h)(1+a')\}^2]\tilde{C}_{m(\alpha)}\tilde{\alpha}_{(w)} + \bar{B}_2 ca_{ac} cos\theta...$$
$$...-\bar{B}_7 ca_{ac} sin\theta$$

$$\bar{B}_{13} = -\tfrac{1}{2}\rho c^2[2\{\Omega(x+h)(1+a')\}]\tilde{C}_m - \tfrac{1}{2}\rho c^2[\{V_0(1-a)\}^2...$$
$$...+\{\Omega(x+h)(1+a')\}^2]\cdot\tilde{C}_{m(\alpha)}\tilde{\alpha}_{(v)} + \bar{B}_3 ca_{ac} cos\theta...$$
$$...-\bar{B}_8 ca_{ac} sin\theta$$

$$\bar{B}_{14} = -\tfrac{1}{2}\rho c^2[\{V_0(1-a)\}^2 + \{\Omega(x+h)(1+a')\}^2]\tilde{C}_{m(\alpha)}\tilde{\alpha}_{(\phi)}...$$
$$...+\bar{B}_4 ca_{ac} cos\theta - \bar{B}_9 ca_{ac} sin\theta$$

$$\bar{B}_{15} = \tfrac{1}{2}\rho c^2[\{V_0(1-a)\}^2 + \{\Omega(x+h)(1+a')\}^2]\cdot\tilde{C}_{m(\alpha)}...$$
$$...+ca_{ac}\{(\bar{B}_5 - \bar{B}_6)cos\theta - (\bar{B}_{10} + \bar{B}_1)sin\theta\}$$

$$\tilde{\alpha} = tan^{-1}\left(\frac{V_0(1-a)}{\Omega(x+h)(1+a')}\right) - \theta$$

$$\tilde{\alpha}_{(w)} = \frac{\Omega(x+h)(1+a')}{\{V_0(1-a)\}^2 + \{\Omega(x+h)(1+a')\}^2}$$

$$\tilde{\alpha}_{(v)} = \frac{-V_0(1-a)}{\{V_0(1-a)\}^2 + \{\Omega(x+h)(1+a')\}^2}$$

$$\tilde{\alpha}_{(\phi)} = \frac{c(\tfrac{1}{4} - a_{ac})\{V_0(1-a)sin\theta + \Omega(x+h)(1+a')cos\theta\}}{\{V_0(1-a)\}^2 + \{\Omega(x+h)(1+a')\}^2}$$

$$\tilde{\alpha}_{(\phi)} = -1$$

$$\tilde{\psi} = \tilde{\alpha} + \theta$$

$$\tilde{\psi}_{(w)} = \tilde{\alpha}_{(w)}$$

$$\tilde{\psi}_{(v)} = \tilde{\alpha}_{(v)}$$

$$\tilde{\psi}_{(\phi)} = \tilde{\alpha}_{(\phi)}$$

$$\tilde{\psi}_{(\phi)} = 0$$